Exploring frustrated spin systems using projected entangled pair states

V. Murg,[1] F. Verstraete,[2] and J. I. Cirac[1]

[1]*Max-Planck-Institut für Quantenoptik, Hans-Kopfermann-Str. 1, D-85748 Garching, Germany*
[2]*Fakultät für Physik, Universität Wien, Boltzmanngasse 3, A-1090 Wien, Austria*

We study the nature of the ground state of the frustrated J_1-J_2 model and the J_1-J_3 model using a variational algorithm based on projected entangled pair states. By investigating spin-spin correlation functions, we observe a separation in parameter regions with long- and short-range order. A direct comparison with exact diagonalizations in the subspace of short-range valence bond singlets reveals that the system is well described by states within this subset in the short-range order regions. We discuss the question whether the system forms a spin liquid, a plaquette valence bond crystal, or a columnar dimer crystal in these parameter regions.

I. INTRODUCTION

Frustrated spin systems have attracted a lot of interest in the last years, because they may possess exotic ground states that are very different from conventional Néel ordered states. Such states are especially intriguing, as connections to high-T_c superconductivity have been put forward.[1] They are usually characterized by a breakdown of long-range order: the system reorganizes in a quantum state where only local antiferromagnetic correlations are present. The class of such states, named short-range valence bond states (SRVB), encompasses a broad range of phases: they range from valence bond crystals (VBC) with broken translational symmetry to pure spin liquids that have all symmetries restored.

Studies of frustrated systems are especially challenging, because quantum Monte Carlo (QMC) studies are hindered by the sign problem[2] and density matrix renormalization group (DMRG) (Refs. 3–5) investigations are hard to perform for systems with dimensionality larger than one. Other methods that have been developed to take on these systems are, for example, the coupled cluster method,[6] DMRG combined with QMC (Ref. 7), and exact diagonalizations within the subspace of SRVB.[8,9] In this paper, we would like to give the recently developed projected entangled pair states (PEPS) algorithm[10,11] a try. This algorithm has already been successfully applied to the Heisenberg antiferromagnet,[10] the Bose-Hubbard model[11] and the frustrated Shastry-Sutherland model.[12]

In the following, we focus on the $J_1-J_2-J_3$ model. We discuss our observations and possible implications. Before that, we give a quick review of the PEPS algorithm in Sec. II. For a thorough explanation of the algorithm, we refer to Refs. 10, 11, and 13. With the implementation of the algorithm, we follow in large part Ref. 11.

II. PEPS ALGORITHM REVISITED

The PEPS algorithm is a variational algorithm within the class of PEPS.[10,11] These states are expedient for a numerical study of many-particle systems; on the one hand, they fulfill the area law that is fundamental to noncritical systems. On the other hand, they possess a number of parameters that scales polynomially with the system size. This feature makes numerical simulations feasible.

The structure of PEPS is inspired from the structure of *matrix product states* (MPS) (Refs. 14 and 15) that form the basis for the successful DMRG algorithm:[3–5] to each lattice site, a tensor is associated that possesses a physical index and a certain number of virtual indices. The virtual indices are contracted according to a scheme that mimics the underlying lattice structure. The dimension of the physical index equals the physical dimension of the particle residing on that lattice site. The dimension of the virtual indices, D, is the internal refinement parameter of PEPS: $D=1$ specializes the PEPS to a product state; the choice $D=d^N$ (with N being the total number of lattice sites and d the physical dimension of one particle) enlarges the space of PEPS to the complete Hilbert space of the system.

The main idea of the algorithm is to optimize the tensors such that the energy tends to a minimum. This can be done by sequentially optimizing the tensors or by cooling the system with the simulation of an imaginary time evolution. Here, we follow the latter. Time and memory required for this method turn out to be polynomial both in N and D: time scales as N^2D^{10} and memory as ND^8 for systems with open boundary conditions. For systems with periodic boundary conditions, scaling requires an additional factor of D^6. This is why we assume open boundary conditions in the following.

This polynomial scaling allows us to investigate systems of sizes that are out of reach with other algorithms. We discuss our observations in the following sections.

III. $J_1-J_2-J_3$ MODEL

In the $J_1-J_2-J_3$ model on a square lattice, frustration is caused by the competition between first-, second-, and third-neighbor interactions of magnitudes J_1, J_2, and J_3, respectively:

$$H = J_1\sum_{\langle ij \rangle} \mathbf{s}_i \cdot \mathbf{s}_j + J_2\sum_{\langle\langle ij \rangle\rangle} \mathbf{s}_i \cdot \mathbf{s}_j + J_3 \sum_{\langle\langle\langle ij \rangle\rangle\rangle} \mathbf{s}_i \cdot \mathbf{s}_j.$$

The phase diagram of this model is involved and still controversial. Of special interest are the regimes of maximal frustration that are suspected of having nonclassical ground states.
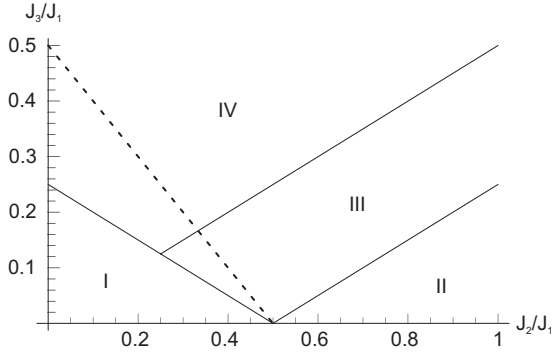
FIG. 1. Classical phase diagram of the $J_1-J_2-J_3$ model consisting of (I) a Néel phase, (II) a phase consisting of two independent sublattices, (III) a helical phase with order (q,q), and (IV) a helical phase with order (q,π). The dashed line denotes the boundary of the Néel phase when quantum fluctuations are taken into account.

Let us first review the classical limit[16–19] ($S \rightarrow \infty$). In this limit, the system possesses four phases, as shown in Fig. 1: the usual Néel phase, two spiral antiferromagnetic phases ordered at (q,q) and (q,π), and a phase consisting of two independent sublattices. The Néel phase is bounded by the *classical critical line* $(J_2+2J_3)/J_1=1/2$.

When quantum fluctuations are taken into account, the phase diagram changes considerably:[8,16,20–22] the Néel phase substantially extends to larger values of J_3, up to the line of maximal frustration $(J_2+J_3)/J_1=1/2$. In the vicinity of this line, it is believed that the classical ordered ground state is destabilized and a singlet ground state is formed.[8] The precise nature of this state is still controversial: suggestions include columnar valence bond crystals,[23] plaquette states,[8] and spin liquids.[24–28] Special attention has been devoted to the end points of the line: the point at $J_3/J_1=1/2$ that separates the Néel from the spiral antiferromagnetic phase[24,26,28] and the tricritial point at $J_2/J_1=1/2$ at which three phases meet.[7,25,27,29]

In the following, we focus on two lines in the phase diagram that include these points: $J_2=0$ (J_1-J_3 model) and $J_3=0$ (J_1-J_2 model). In both cases, we apply the PEPS algorithm and discuss our observations. Our investigations are thereby inspired by the discussions in Ref. 8. We obtain the PEPS approximation of the ground state via imaginary time evolution, as described previously. Imaginary time evolution is very stable and always tends to the global minimum, independent of the starting state. In the course of the time evolution, we increase the virtual dimension D, starting from $D=2$, and decrease the Trotter step δt, starting from $\delta t=0.03/J_1$, until the relative changes in the ground state energy are of order 10^{-3}. This is usually achieved for $D=4$ and $\delta t=0.003/J_1$. Typically, $D=4$ only leads to a minor reduction in the energy. The energy as a function of the imaginary time evolution steps is plotted in Fig. 2 for the special case of a 10×10 lattice and $J_3/J_1=0.5$.

A. Spin-spin correlations

In order to get a first idea of the nature of the ground state, we calculate the spin-spin correlation functions $\langle \mathbf{s}_k \cdot \mathbf{s}_l \rangle$ and the corresponding static structure factor,
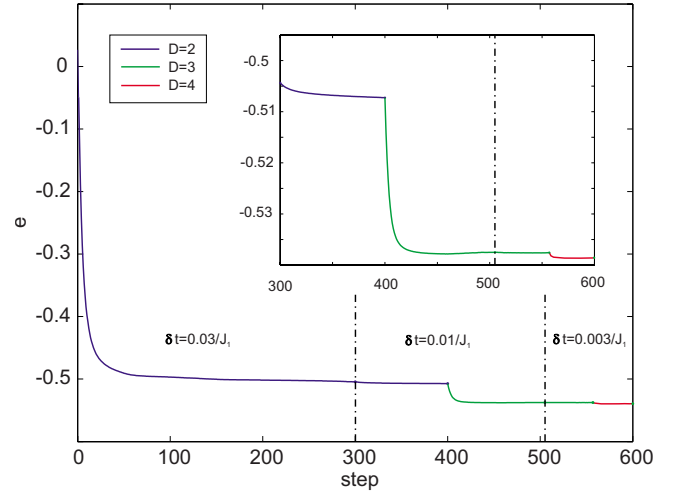

FIG. 2. (Color online) Energy per site as a function of the imaginary time evolution steps. The lattice size is 10×10 and $J_3/J_1 = 0.5$. The inset shows the magnified tail of the energy function. The vertical lines separate the plot into three regions: in these regions, the Trotter step δt is chosen equal to $0.03/J_1$, $0.01/J_1$, and $0.003/J_1$, respectively.

$$S(\mathbf{q}) = \frac{1}{N^2} \sum_{kl} e^{i\mathbf{q} \cdot (\mathbf{r}_k - \mathbf{r}_l)} \langle \mathbf{s}_k \cdot \mathbf{s}_l \rangle, \qquad (1)$$

in the PEPS approximation of the ground state for $0 \leq J_3/J_1 \leq 1$ at $J_2=0$ and $0 \leq J_2/J_1 \leq 1$ at $J_3=0$.

1. J_1-J_3 model

In the case of $J_2=0$, we observe that $S(\mathbf{q})$ is peaked at $\mathbf{q}=(\pi,\pi)$ for $J_3/J_1 < 0.5$, indicating long-range Néel order. This order disappears at $J_3/J_1 \sim 0.5$ at which the structure factor becomes smooth. At around $J_3/J_1 \sim 0.7$ peaks at $(\pm\pi/2, \pm\pi/2)$ reappear indicating a revival of incommensurate long-range order. Figure 3 depicts the functional characteristics of the structure factor $S(\mathbf{q})$ at selected points J_3/J_1
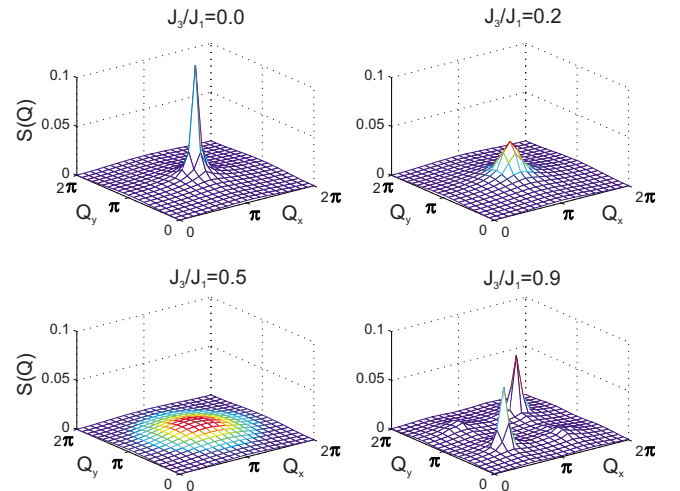

FIG. 3. (Color online) Structure factor $S(\mathbf{q})$ for $J_3/J_1=0$, 0.2, 0.5, and 0.9. The results were obtained for a 14×14 lattice and virtual dimension $D=3$.

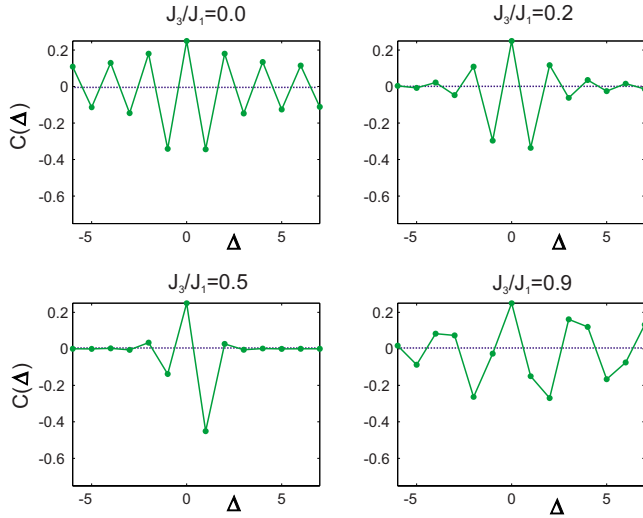FIG. 4. (Color online) Spin-spin correlations $\langle \mathbf{s}_i \cdot \mathbf{s}_j \rangle$ as functions of the distance $\Delta = |i - j|$ for the $14 \times 14 J_1 - J_3$ model at $J_3/J_1 = 0$, 0.2, 0.5, and 0.9. The results have been obtained using a $D=3$ PEPS ansatz.

calculated with a $D=3$ PEPS on a 14×14 lattice.

The collapse of long-range order is confirmed by a direct observation of the spin-spin correlations. These are shown in Fig. 4. Here, correlations with the central spin are plotted as functions of the distance. As can be seen, the spins are antiferromagnetically ordered for $J_3/J_1 < 0.5$. For $J_3/J_1 > 0.5$, every second spin possesses antiferromagnetic order. However, the long-range order of the spins disappears in the vicinity of $J_3/J_1 \sim 0.5$.

The separation in long- and short-range order regimes gets more and more evident with growing number of sites. This can be gathered from Fig. 5. Here, $S(\pi, \pi)$ and $S(\pi/2, \pi/2)$ are plotted as functions of J_3/J_1, evaluated for various numbers of sites N. An extrapolation to the thermo-
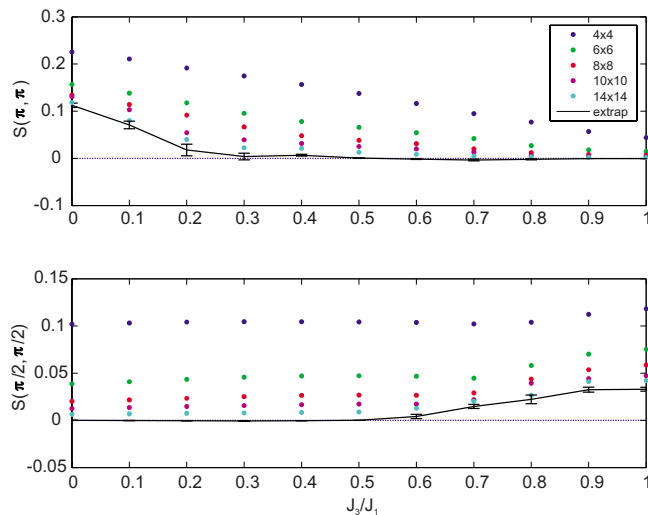

FIG. 5. (Color online) Structure factors $S(\pi, \pi)$ (upper plot) and $S(\pi/2, \pi/2)$ (lower plot) as functions of J_3/J_1 for various numbers of sites N. The solid lines represent extrapolations to the thermodynamic limit (see text).
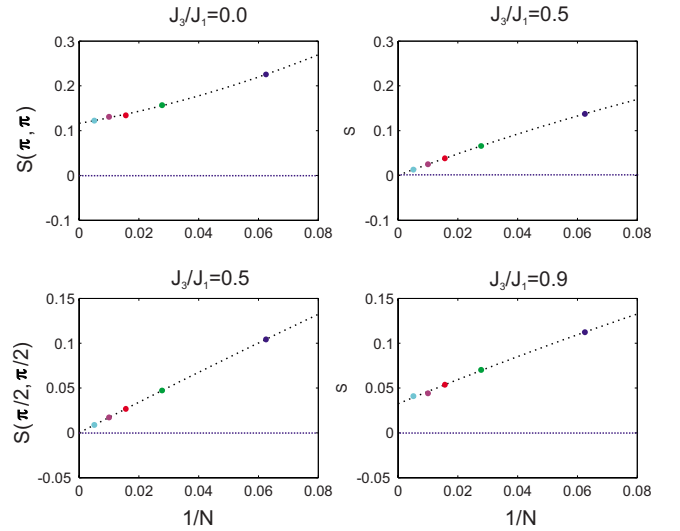

FIG. 6. (Color online) Structure factors $S(\pi, \pi)$ (upper plots) and $S(\pi/2, \pi/2)$ (lower plots) as functions of $1/N$ for selected points J_3/J_1. The dotted lines represent the best fits by polynomials of degree 3 in $1/N$.

dynamic limit $(N \rightarrow \infty)$ shows that $S(\pi, \pi)$ remains finite within the region $J_3/J_1 \lesssim 0.3$ and is zero otherwise. On the other hand, $S(\pi/2, \pi/2)$ is zero up to $J_3/J_1 \sim 0.7$ and finite for larger values of J_1/J_3. The region of short-range order is thus narrowed down to $0.3 \lesssim J_3/J_1 \lesssim 0.6$.

The extrapolation was obtained by fitting a polynomial of degree 3 in $1/N$ to values of $S(\mathbf{q})$ for various values of N. The error bars in the plot indicate the error estimates for the predictions. The data points are usually fitted very well with such a polynomial as can be seen in Fig. 6. In this figure, for selected points J_3/J_1, the scaling of $S(\mathbf{q})$ with N is plotted and the best fit by a polynomial of third degree in $1/N$ is drawn. From this fit, we obtain the predictions for the thermodynamic limit.

2. $J_1 - J_2$ model

For $J_3 = 0$, the static structure factor shows the following behavior: for $J_2/J_1 \lesssim 0.5$ the structure factor is peaked at (π, π) which indicates long-range Néel order. For J_2/J_1 larger than 0.5, columnar long-range order develops which is detected by a peak at $(0, \pi)$. In fact, this columnar long-range order reveals an order by disorder phenomenon:[30] quantum fluctuations select from the huge manifold of classical ground states configurations where all spins are parallel in a given direction. In the regime in between the Néel and the columnar phase the peaks disappear and long-range order breaks down. The structure factor obtained from the PEPS calculation for $D=3$ and a 14×14 lattice is plotted in Fig. 7 for selected values of J_2/J_1.

In Fig. 8, $S(\pi, \pi)$ and $S(\pi, \mathbf{0})$ are plotted as functions of J_2/J_1 for various numbers of sites N. The extrapolation to the thermodynamic limit indicates that $S(\pi, \pi)$ remains finite for $J_2/J_1 \lesssim 0.5$, and that $S(\pi, \mathbf{0})$ is finite for $J_2/J_1 \gtrsim 0.5$. Thus, the systems consists of two phases with long-range order plus a possibly very small short-range order phase in the vicinity of $J_2/J_1 \sim 0.5$.
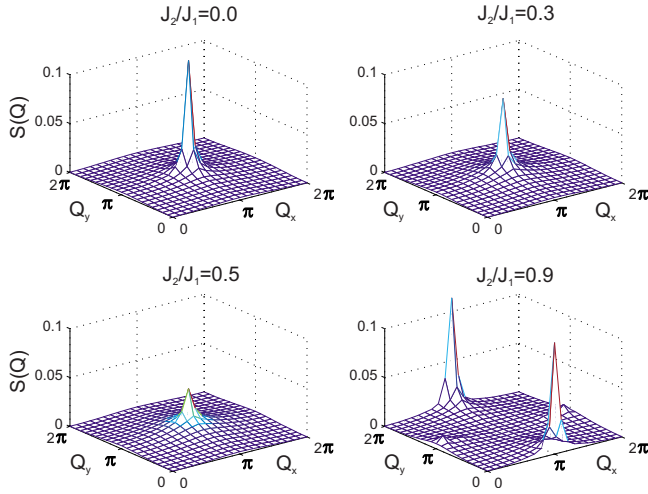
FIG. 7. (Color online) Structure factor $S(\mathbf{q})$ for J_2/J_1 equal to 0, 0.3, 0.5, and 0.9. The results were obtained for a 14×14 lattice and $D=3$.

IV. SHORT-RANGE RESONATING VALENCE BOND STATES

The considerable decrease in the correlation length at $J_3/J_1 \sim 0.5$ and $J_2/J_1 \sim 0.5$ opens the possibility for a short-range resonating valence bond state (SRVB) in this area. We investigate this possibility by doing a direct comparison of the PEPS results to results obtained by an exact diagonalization of the Hamiltonian in the subspace of SRVB.

A. $J_1 - J_3$ model

In case of the $J_1 - J_3$ model, the overlap between the SRVB and the PEPS with virtual dimensions $D=3$ on a 6×6 lattice can be gathered from Fig. 9 (lower plot). As it can
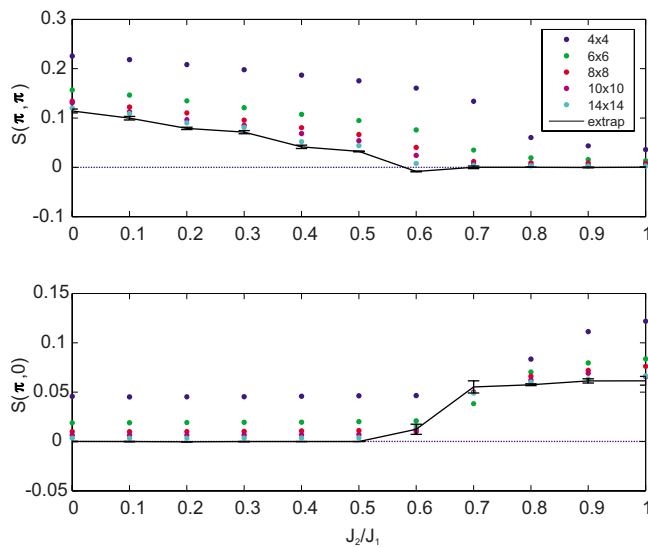

FIG. 8. (Color online) Structure factors $S(\pi, \pi)$ (upper plot) and $S(\pi, \mathbf{0})$ (lower plot) as functions of J_2/J_1 for various numbers of sites N. The solid lines represent extrapolations to the thermodynamic limit.
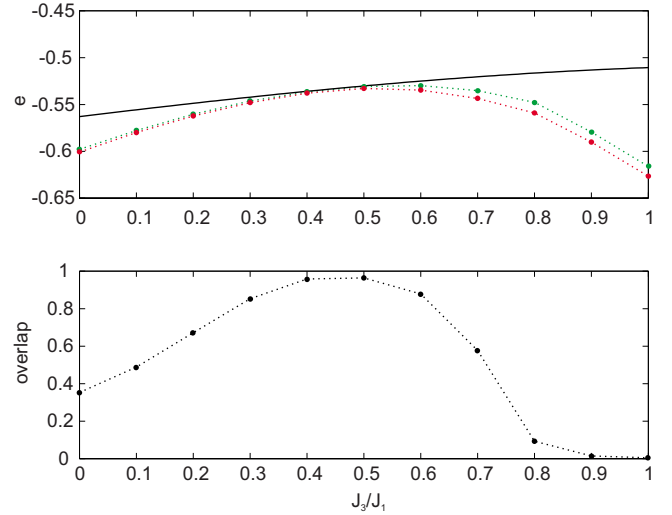

FIG. 9. (Color online) Upper plot: Ground state energy of the $J_1 - J_3$ model on a 6×6 lattice as a function of J_3/J_1 obtained by diagonalizing within the SRVB subspace (solid line) and by PEPS calculations with $D=3$ (upper dotted line) and $D=4$ (lower dotted line). Lower plot: Overlap between the SRVB ground state and the $D=3$ PEPS ground state.

be seen, the overlap increases up to 99% at the point $J_3/J_1 = 0.5$ and is significantly smaller in other regions. A comparison of energies, however, reveals that the set of valence bond states does not cover all terms in the ground state. As shown in the upper plot of Fig. 9, the energies of the diagonalization within the subspace of SRVB are though very close to the PEPS results at $J_3/J_1 \sim 0.5$, always higher than the energies obtained within the set of PEPS. Thus, the true ground state at $J_3/J_1 \sim 0.5$ might contain a small fraction of valence bond terms that have longer range.

Even if it is assumed that the ground state is a pure SRVB in the vicinity of $J_3/J_1 = 0.5$, its properties can be very rich and it needs a more precise classification. On the one hand, it could be a state with broken translational symmetry such as a columnar valence bond crystal or a plaquette state. On the other hand, an equally weighted superposition of valence bond states with restored translational symmetry known as spin liquid is possible.

The observation of nearest-neighbor spin-spin correlations $\langle \mathbf{s}_i \cdot \mathbf{s}_j \rangle$ gives us an indication of a plaquette state.[31] These correlations are shown in Fig. 10 for a 8×8 lattice and $D=3$. In case of a pure plaquette state, the nearest-neighbor spin-spin correlations would be equal to $-1/2$ on a plaquette and 0 between two plaquettes. In our case, the values of the spin-spin correlations deviate slightly from these values, nonetheless a clear plaquette structure remains visible.

The state we observe has obviously a broken translational symmetry. The plaquettes are formed between sites (i, j), $(i+1, j)$, $(i, j+1)$, $(i+1, j+1)$, with i and j always being odd. The reason for this symmetry breaking is the chosen open boundary conditions and the even number of sites in x and y directions. The system chooses the configuration with a maximal number of plaquettes. In case of open boundary conditions and an even number of sites in each direction, this
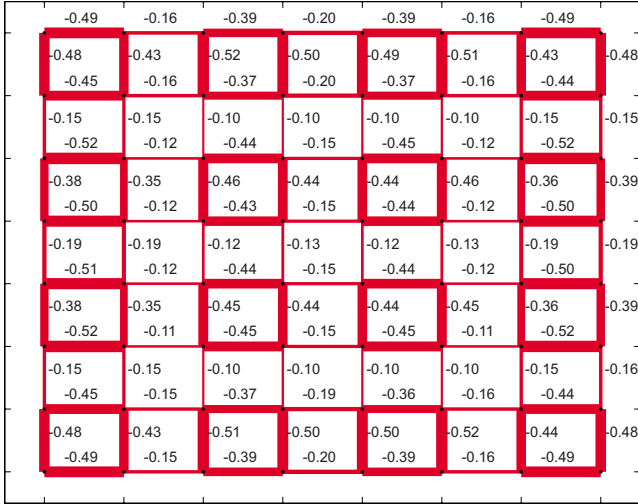
FIG. 10. (Color online) Nearest-neighbor spin-spin correlations at $J_3/J_1=0.5$, calculated with $D=3$ PEPS.

FIG. 12. (Color online) Nearest-neighbor spin-spin correlations at $J_2/J_1=0.6$, calculated with $D=3$ EPS.

corresponds to the configuration of plaquettes with i and j being odd.

B. J_1-J_2 model

The vicinity of the ground state to the class of SRVB in the region $J_2/J_1 \sim 0.5$ is analyzed in Fig. 11. The lower plot shows the overlap of the PEPS ground state with the ground state obtained by exact diagonalization within the PEPS subspace. Lattice size 6×6 and virtual dimensions $D=3$ were considered. The overlap clearly reaches the maximum at $J_2/J_1=0.5$ and assumes a value of about 70%. A comparison of the energies, as shown in the upper plot of Fig. 11, uncovers that the true ground state will not be exactly in the sub-
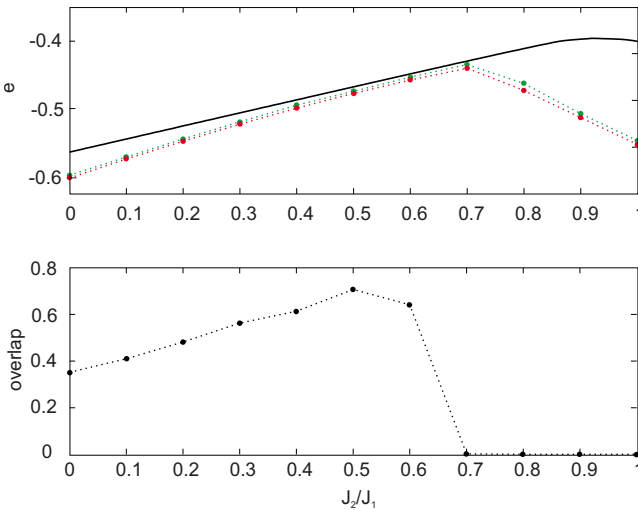
space of SRVB: the energies of the PEPS calculations are slightly lower than the ones obtained from SRVB, even at the critical point. Nonetheless, the distance to the subspace of SRVB might be very small for $J_2/J_1 \sim 0.5$.

A more precise classification of the ground state turns out to be more difficult than in the case of the J_1-J_3 model: observations of the nearest-neighbor spin-spin correlations $\langle \mathbf{s}_i \cdot \mathbf{s}_j \rangle$ yield faint indications for a columnar dimer state.[23] The magnitudes of the nearest-neighbor spin-spin correlations for a 8×8 lattice, $D=3$ and $J_2/J_1=0.6$ are shown in Fig. 12. In a pure dimer state, the spin-spin correlations are equal to $-3/4$ on a dimer bond and zero between two dimer bonds. Even though these values are not attained, a columnar order of dimers is visible.

V. OTHER ORDER PARAMETERS

In order to shed more light on the properties of the ground state in the maximally frustrated regime, more elaborate order parameters are investigated such as the plaquette order parameter,[31] the columnar order parameter, or the VBC order parameter.[8]

The plaquette order parameter[31] distinguishes clearly a Néel ordered phase from a plaquette valence bond crystal. It is defined, using the cyclic permutation operator $P_{\alpha\beta\gamma\delta}$ of the four spins α, β, γ, and δ on one plaquette, as

$$Q_{\alpha\beta\gamma\delta} = \frac{1}{2}(P_{\alpha\beta\gamma\delta} + P_{\alpha\beta\gamma\delta}^{-1}) = 2(\mathbf{s}_\alpha \cdot \mathbf{s}_\beta \mathbf{s}_\gamma \cdot \mathbf{s}_\delta + \mathbf{s}_\alpha \cdot \mathbf{s}_\delta \mathbf{s}_\beta \cdot \mathbf{s}_\gamma$$

$$- \mathbf{s}_\alpha \cdot \mathbf{s}_\gamma \mathbf{s}_\beta \cdot \mathbf{s}_\delta) + \frac{1}{2}(\mathbf{s}_\alpha \cdot \mathbf{s}_\beta + \mathbf{s}_\gamma \cdot \mathbf{s}_\delta + \mathbf{s}_\alpha \cdot \mathbf{s}_\delta + \mathbf{s}_\beta \cdot \mathbf{s}_\gamma)$$

$$+ \frac{1}{2}(\mathbf{s}_\alpha \cdot \mathbf{s}_\gamma + \mathbf{s}_\beta \cdot \mathbf{s}_\delta + 1/4).$$

In case of a pure plaquette state, this order parameter assumes the value 1 on each plaquette; between the plaquettes, its expectation value is 1/8. The order parameter vanishes in

FIG. 11. (Color online) Upper plot: Ground state energy of the J_1-J_2 model on a 6×6 lattice as a function of J_2/J_1, obtained by diagonalizing within the SRVB subspace (solid line) and by PEPS calculations with $D=3$ (green dots) and $D=4$ (red dots). Lower plot: Overlap between the SRVB ground state and the $D=3$ PEPS ground state.
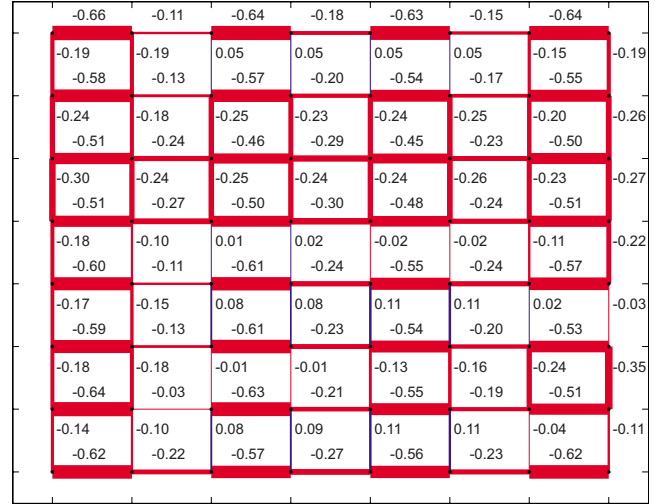
FIG. 13. (Color online) Plaquette order parameter $Q_{\alpha\beta\gamma\delta}$ at $J_3/J_1=0.5$, evaluated on a 8×8 lattice. The used virtual dimension is $D=3$.

case of the Néel state which lacks the cyclic permutation symmetry.

The columnar order parameter and the VBC order parameter[8] are defined as structure factors of dimmer-dimer correlations:

$$S_\lambda = \frac{1}{N_B} \sum_{(k,l)} \varepsilon_\lambda(k,l) [\langle (\mathbf{s}_i \cdot \mathbf{s}_j)(\mathbf{s}_k \cdot \mathbf{s}_l) \rangle - \langle (\mathbf{s}_i \cdot \mathbf{s}_j) \rangle^2].$$

Here, k and l run over all pairs of neighboring sites. i and j have fixed values and they point to two neighboring sites at the center of the lattice. λ represents either "col" or "VBC" and the phase factor $\varepsilon_\lambda(k,l)$ is defined according to Fig. 7 in Ref. 8. N_B denotes the number of terms with $\varepsilon_\lambda(k,l) \neq 0$. As discussed in Ref. 8, S_{VBC} and S_{col} show a different behavior in the plaquette and the columnar dimer phase: in the plaquette phase, S_{VBC} remains finite in the thermodynamic limit and S_{col} tends to zero, whereas in the columnar dimer phase, both S_{VBC} and S_{col} remain finite.

All these order parameters are based on dimmer-dimer correlations which are difficult to obtain with high precision from PEPS calculations. Nonetheless, our results give a qualitative picture of the ground state.

A. J_1-J_3 model

In Fig. 13, we plot the plaquette order parameter evaluated on all square clusters for $J_3/J_1=0.5$ and a 8×8 lattice. The results are obtained using a PEPS ansatz with $D=3$. A clear plaquette structure is visible, though the absolute values of the expectation values differ slightly from the optimal ones.

In Fig. 14, both structure factors S_{VBC} and S_{col} are plotted as functions of J_3/J_1 for various lattice sizes. The values were obtained from a PEPS simulation with $D=3$. The solid lines indicate extrapolations to the thermodynamic limit ($N \to \infty$). The extrapolations were obtained by fitting polynomials of first degree in $1/N$. It can be seen that S_{VBC} is clearly
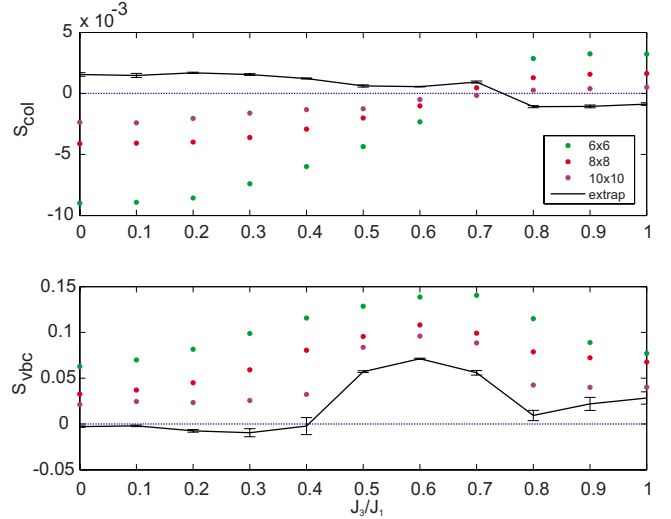

FIG. 14. (Color online) Structure factors S_{col} and S_{VBC} as functions of J_3/J_1 for lattice sizes 6×6, 8×8, and 10×10, calculated using PEPS with $D=3$. The solid lines represent extrapolations to the thermodynamic limit.

peaked in the region $0.4 \lesssim J_1/J_3 \lesssim 0.8$. In addition, S_{col} is 3 orders of magnitude smaller than S_{VBC} in this region. This gives us an indication for a plaquette state in the region $0.4 \leq J_1/J_3 \leq 0.8$.

Thus, the PEPS algorithm reproduces well the properties of the J_1-J_3 model in the regimes of weak frustration and gives strong indications for a plaquette ordered state in the regime of strong frustration. In this regime, our results are consistent with those of Ref. 8.

B. J_1-J_2 model

In Fig. 15, the structure factors S_{VBC} and S_{col} as functions of J_2/J_1 are plotted for various lattice sizes. The virtual di-
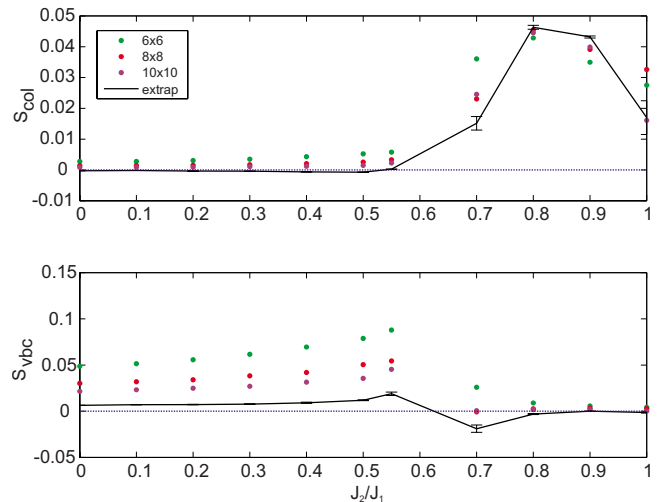

FIG. 15. (Color online) Structure factors S_{col} and S_{VBC} as functions of J_2/J_1 for lattice sizes 6×6, 8×8, and 10×10, calculated using PEPS with $D=3$. The solid lines represent extrapolations to the thermodynamic limit.

mension used for the PEPS simulation was $D=3$. Again, the solid lines represent extrapolations to the thermodynamic limit. As can be seen, both quantities feature regions in which they are finite and regions in which they tend to zero rapidly. In the case of S_{col}, the structure factor is very small for $J_2/J_1 \lesssim 0.5$ and finite otherwise. On the other hand, S_{VBC} is finite for $J_2/J_1 \lesssim 0.7$ and close to zero otherwise. This indicates the existence of a columnar dimer phase within the region $0.5 \lesssim J_2/J_1 \lesssim 0.7$.

VI. CONCLUSIONS

In conclusion, we have applied the PEPS algorithm to the J_1-J_2 and J_1-J_3 models and discussed our observations. In both models we observed a separation in long- and short-range order regions. In the short-range order regions, the ground state seems to lie within the subspace of SRVB states. Due to lack of precision we cannot settle the question of whether the ground state is a VBC or a spin liquid, but there are strong indications that the ground state is a plaquette state in case of the J_1-J_3 model and a columnar dimer state in case of the J_1-J_2 model. Simulations with higher D and the inclusion of symmetries might lead to a more concrete answer.

[1] P. W. Anderson, Science **235**, 1196 (1987).

[2] M. Troyer and U. J. Wiese, Phys. Rev. Lett. **94**, 170201 (2005).

[3] S. R. White, Phys. Rev. Lett. **69**, 2863 (1992).

[4] S. R. White, Phys. Rev. B **48**, 10345 (1993).

[5] U. Schollwöck, Rev. Mod. Phys. **77**, 259 (2005).

[6] J. Richter, R. Darradi, R. Zinke, and R. F. Bishop, Int. J. Mod. Phys. B **21**, 2273 (2007).

[7] M. S. L. du Croo de Jongh, J. M. J. van Leeuwen, and W. van Saarloos, Phys. Rev. B **62**, 14844 (2000).

[8] M. Mambrini, A. Läuchli, D. Poilblanc, and F. Mila, Phys. Rev. B **74**, 144422 (2006).

[9] M. Mambrini and F. Mila, Eur. Phys. J. B **17**, 651 (2000).

[10] F. Verstraete and J. I. Cirac, arXiv:cond-mat/0407066 (unpublished).

[11] V. Murg, F. Verstraete, and J. I. Cirac, Phys. Rev. A **75**, 033605 (2007).

[12] A. Isacsson and O. F. Syljuasen, Phys. Rev. E **74**, 026701 (2006).

[13] F. Verstraete, J. I. Cirac, and V. Murg, Adv. Phys. **57**, 143 (2008).

[14] S. Östlund and S. Rommer, Phys. Rev. Lett. **75**, 3537 (1995).

[15] J. Dukelsky, M. A. Martin-Delgado, T. Nishino, and G. Sierra, Europhys. Lett. **43**, 457 (1998).

[16] J. Ferrer, Phys. Rev. B **47**, 8769 (1993).

[17] A. Chubukov, Phys. Rev. B **44**, 392 (1991).

[18] A. Moreo, E. Dagotto, T. Jolicoeur, and J. Riera, Phys. Rev. B **42**, 6283 (1990).

[19] M. P. Gelfand, R. R. P. Singh, and D. A. Huse, Phys. Rev. B **40**, 10801 (1989).

[20] F. Figueirido, A. Karlhede, S. Kivelson, S. Sondhi, M. Rocek, and D. S. Rokhsar, Phys. Rev. B **41**, 4619 (1990).

[21] N. Read and S. Sachdev, Phys. Rev. Lett. **66**, 1773 (1991).

[22] S. Sachdev and N. Read, Int. J. Mod. Phys. B **5**, 219 (1991).

[23] P. W. Leung and N. W. Lam, Phys. Rev. B **53**, 2213 (1996).

[24] L. Capriotti, D. J. Scalapino, and S. R. White, Phys. Rev. Lett. **93**, 177004 (2004).

[25] Q. F. Zhong and S. Sorella, Europhys. Lett. **21**, 629 (1993).

[26] L. Capriotti and S. Sachdev, Phys. Rev. Lett. **93**, 257206 (2004).

[27] P. Chandra and B. Doucot, Phys. Rev. B **38**, 9335 (1988).

[28] P. Locher, Phys. Rev. B **41**, 2537 (1990).

[29] P. Chandra, P. Coleman, and A. I. Larkin, Phys. Rev. Lett. **64**, 88 (1990).

[30] J. Villain, J. Phys. (Paris) **38**, 385 (1977).

[31] J. B. Fouet, M. Mambrini, P. Sindzingre, and C. Lhuillier, Phys. Rev. B **67**, 054411 (2003).